Turkish Journal of Electrical Engineering & Computer Sciences

http://journals.tubitak.gov.tr/elektrik/

Research Article

Turk J Elec Eng & Comp Sci
(2021) 29: 1044 – 1060

doi:10.3906/elk-2005-206

A nonlinear disturbance observer scheme for discrete time control systems

Mehmet Önder EFE[1,*], **Coşku KASNAKOĞLU**[2]
[1]Department of Computer Engineering, Faculty of Engineering, Hacettepe University, Ankara, Turkey
[2]Department of Electrical and Electronics Engineering, Faculty of Engineering,
TOBB University of Economics and Technology, Ankara, Turkey

Received: 02.06.2020 • **Accepted/Published Online:** 24.08.2020 • **Final Version:** 30.03.2021

Abstract: This paper presents a modification to the original disturbance observer based control (DOBC) scheme by redefining the lowpass filter using a nonlinear element. The proposed technique improves the disturbance prediction performance for both small and large magnitude disturbance signals. The contribution of the current work is to unfold the stability and performance conditions under the proposed modification. A comparative set of simulation studies are discussed and it is seen that the proposed modification results in smaller disturbance prediction error energy and smaller tracking error energy when the plant model is discrete time and uncertain.

Key words: Discrete time disturbance observer, robust control, nonlinear Q-filter, S-filter

1. Introduction

Robust control of systems having time delays has been an important research problem for many years [1–3] and disturbance observers have constituted effective solutions to the problem. Disturbance observer based control (DOBC) has been very popular during the last two decades and many contributions to the field have been made. Among them, the contributions considering the continuous time case are remarkably more in number than those in discrete time. Typical DOBC structure entailing the inverse model of the nominal system dynamics requires the selection of an appropriate lowpass filter that predicts the disturbance within its bandwidth. This obviously necessitates a minimum phase nominal plant model. Causality of the inverse model is another requirement that can be met using serially connected lowpass components to obtain a causal inverse model.

The disturbance observer mechanism utilizing the inverse model adopts the same block structure as we have in continuous time. The fundamental question here is whether it is possible to predict the disturbance signal and remove it from the loop up to a particular frequency. The overall control system has two inputs, the reference signal and the disturbance signal, and the system has two outputs, namely, the plant output and the predicted disturbance. The goal in both continuous and discrete time implementation is to obtain a lowpass characteristic for disturbance signal to predicted disturbance and reference signal to plant output. This is necessary for command tracking and disturbance cancellation. Further, the control system must suppress the coupling terms, i.e. the relation from disturbance to plant output and reference signal to predicted disturbance signal. A DOBC discussion must contain these issues together with the uncertainty types and associated stability conditions. In the literature, several works have been reported towards the goal of suppressing adverse effects of the disturbances. In [1], acceleration feedback is used for enhancing the disturbance rejection quality.

*Correspondence: onderefe@gmail.com

The disturbance prediction subsystem is implemented in discrete time and the technique is studied for AC machines. In another study, the disturbance observation problem has been considered in the framework of neural network aided model predictive control in discrete time in [2], where the goal is to follow constant reference signals with zero steady state error. The disturbance observer problem for telerobotic systems is studied in [3], where the transmission delay is considered as a difficulty to be alleviated and a continuous time approach with Smith predictor is developed. The notion of continuous time DOBC was introduced for the first time by Prof. Ohnishi in [4]. The stability and performance issues have stayed at the center of the discussions and a number of surveys have been reported to update the most recent literature and developments in theory and practice [5, 6]. Considering the continuous time systems, the cited volume of literature in [5, 6] address a fairly wide spectrum yet the issues of discrete time implementations still need further research as the difficulties introduced by sampling and coexistence of the digital hardware together with the continuous time systems survive persistently.

In [7], plants having pure delay were studied by Kempf and Kobayashi and the disturbance observer block diagram is modified according to the available dead time, uncertainty on which adversely influences the performance as the block structure is modified according to the available amount of dead time for best performance. In [8], Godler et al. studied the effects of the sampling time on the performance and robustness for speed control systems and the work emphasizes that the sampling frequency is an essential parameter for discrete time DOBC systems. In [9], Yang et al. elaborated the effects of measurement noise on the disturbance rejection performance. A set of guidelines for designing the Q-filter has been proposed and discretization was done by using bilinear transformation. One of the guidelines given in this work highlights choosing a high order numerator polynomial for the lowpass filter Q. Another guideline in [9] recommends using a Q-filter having small time constant to obtain a better disturbance prediction performance. In [10], a cascaded frequency shaping filter is introduced into the classical disturbance observer loop to avoid adverse effects of resonance modes. This modification provides an increase in the bandwidth of the Q-filter and an enhanced closed loop performance is obtained. Lee et al. reported the relation between the time constant of Q-filter and the sampling period and delay function is proposed as the new Q-filter [11], where necessary condition for stability and robustness is discussed. Linear matrix inequality approach is used to predict the state and input/output disturbances for discrete time models in [12]. In [13, 14], a sampled data system together with a discrete time DOB is considered and an almost necessary and sufficient condition for robust stability is given when there is fast sampling. In the work reported by Yun et al. [15], the zeros caused by sampling are paid special care and using the discrete-time singular perturbation theory, a robust stability condition is derived for state space models. In [16], a fundamental issue of discrete time DOBC is considered. Three discretization approaches, namely, backward difference method, bilinear transformation and and Al-Aloui discretization method are comparatively studied in terms of closed loop performance based on integral of the absolute error criterion. The work advises using bilinear transformation as the operator for discretization. The work of Muramatsu and Katsura [17] considers removing the periodic disturbances using the fundamental wave and harmonics with a time-delay element. The approach uses the inverse of the nominal model as we adopt in this work.

This paper considers a modification to the classical lowpass filter, the Q-filter, that is used to remove the algebraic loop problem as well as the possible spurious spectral content in the input signal. The proposed approach inserts a nonlinear element into the so called Q-filter and the obtained nonlinear filter, which is called S-filter, becomes sensitive to small magnitude disturbance values making the overall DOBC performance superior to the conventional setting. The current paper differentiates from the existing body of literature in

terms of i) a thorough analysis of the classical case considering the discrete time conditions, ii) a nonlinear term for improving the response, and iii) an in depth analysis of stability and performance for the proposed approach. The contribution of this work is to postulate a DOBC mechanism that operates in discrete time with comparably high performance and with a minor modification to the conventional approach.

This paper is organized as follows: Section 2 provides the analysis of the discrete time DOBC scheme in the classical setting, and Section 3 provides the theoretical and analytical aspects of the proposed scheme. The justifying work with a comparison to the classical approach is presented in Section 4 and the concluding remarks emphasizing the contributions are given at the end of the paper.

2. Unfolding the facts of classical discrete time disturbance observer based control

Consider the classical DOBC block diagram shown in Figure 1a with all blocks are discretized properly. In this figure, $P(z)$ is the uncertain plant, $P_n(z)$ is the known nominal plant model, $Q(z)$ is a low pass filter (the Q-filter), $C(z)$ is a controller that yields the desired closed loop response when $P(z) = P_n(z)$, $R(z)$ is the command signal, $D(z)$ is the disturbance signal and $X(z)$ is the measurement noise. The auxiliary variables shown in the figure are $\hat{D}(z)$ for the predicted value of the disturbance signal and $U(z)$ for the computed control signal.

It is straightforward to write the following relation that characterizes the output of the control system. For simplicity, we will drop the argument z and proceed as follows: $Y = \frac{P}{1+Q(PP_n^{-1}-1)}U + \frac{P(1-Q)}{1+Q(PP_n^{-1}-1)}D - \frac{QPP_n^{-1}}{1+Q(PP_n^{-1}-1)}X$

If the stability and causality (physical realizability) conditions are met, the loop shown in Figure 1a provides a useful approximate of the disturbance D and removes its adverse effects by subtracting its estimate $\hat{D}$ from the control signal. An important issue that was considered extensively in the literature is the selection of the bandwidth of the Q-filter, which influences the closed loop performance to some extent.

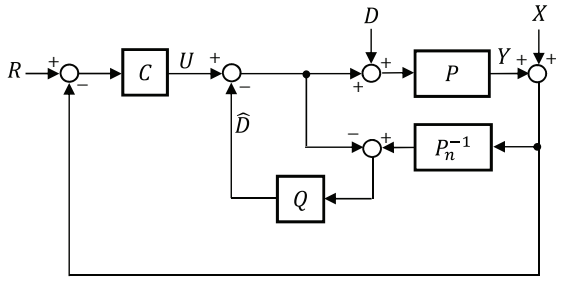

(a) Block diagram of the Q-filter based classical continuous time DOBC scheme, where Q is a first order low pass filter given as $Q(s) = \frac{K}{s+K}$ and $K > 0$.

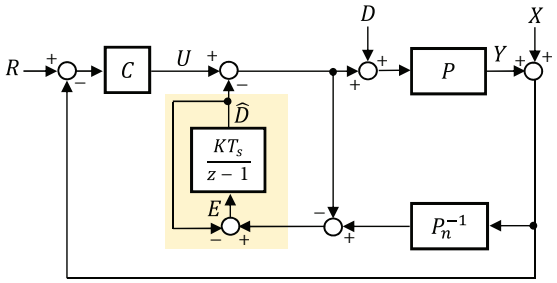

(b) Expanded view of the structure in Figure 1a with the discretization $\mathcal{Z}\{\frac{K}{s}\} = \frac{KT_s}{z-1}$, where T_s is the sampling period.

Figure 1. Classical block diagram and reinterpretation of it.

Now we expand the Q-filter and use a discrete time integrator as shown in Figure 1b, where T_s is the sampling period and $K > 0$ is a gain, the conditions over which will be discussed in the sequel. Considering the shaded area in Figure 1b, the first condition for stability is $|-1+KT_s| < 1$, which leads to $0 < KT_s < 2$ for the subsystem producing the signal $\hat{D}$.

Considering the outer loop, two fundamental equations can be derived from Figure 1b, and these equations are given as

$$U = \frac{C}{1+PC}R - \frac{PC}{1+PC}(D-\hat{D}) - \frac{C}{1+PC}X, \tag{1}$$

$$E = \frac{(PP_n^{-1}-1)C}{1+PC}R + \frac{PP_n^{-1}+PC}{1+PC}(D-\hat{D}) + NX, \tag{2}$$

where $N := P_n^{-1}\frac{1+P_nC}{1+PC}$. According to the diagram shown in Figure 1b, the sensitivity transfer function can be defined as $S := \frac{1}{1+PC}$, the complementary sensitivity transfer function can be defined as $T := 1-S = \frac{PC}{1+PC}$. Also, we define $T_n := \frac{P_nC}{1+P_nC}$ as the nominal closed loop transfer function and ω_{T_n} as the bandwidth associated to it.

Let $\tilde{\Delta}(z)$ stand for an unknown transfer function such that $\|\tilde{\Delta}\|_\infty \leq 1$ and let W denote a real rational transfer function.

In Figure 1b, the input signal to the block with transfer function $\frac{KT_s}{z-1}$ is denoted by E, and using (1) and (2), the general expression for E can be obtained as in (3)

$$E = GCR + (1+G)(D-\hat{D}) + NX, \tag{3}$$

where the transfer function $G := \frac{PP_n^{-1}-1}{1+PC}$ is defined in the table for four fundamental uncertainty types and it is independent of K. According to Figure 1b, the quantity denoted by E passes through the block $KT_s/(z-1)$ and the obtained output is $\hat{D}$. An equivalent block diagram implementing (3) is illustrated in Figure 2a. In order to analyze the stability of the equivalent feedback loop shown in Figure 2a, we will assume $R \equiv X \equiv 0$. In Figure 2b, we redraw the $1+G$ term explicitly with zero external excitations and small gain theorem becomes applicable to the shown loop. It is straightforward to derive $\frac{u_G}{y_G} = -Q = -\frac{KT_s}{z-1+KT_s}$ and the necessary condition for stability is to choose $\|-Q\|_\infty < 1 \Rightarrow 0 < KT_s < 1$ if $\|G\|_\infty < 1$ holds true.

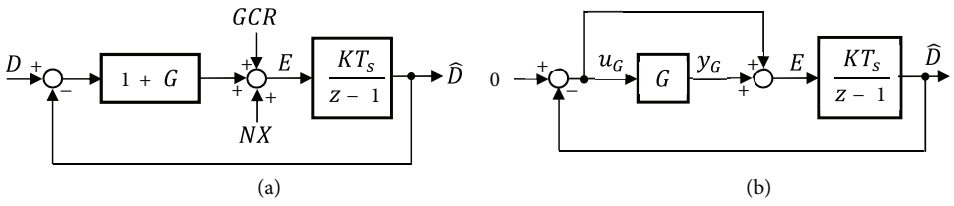

Figure 2: (a) Equivalent representation of the disturbance prediction loop, (b) small gain theorem compatible representation of the disturbance prediction loop.

Alternatively, considering Figure 2a with $R \equiv X \equiv 0$, we assume that the open loop transfer function $G_{OL} := (1+G)\frac{KT_s}{z-1}$ has no unstable poles. At the verge of instability, we know that $1+G_{OL}(e^{j\omega_{cr}T_s}) = 0$, where ω_{cr} is the frequency at which the closed loop system has poles on the unit circle and self sustained

Table . Types of uncertainty and corresponding $G(z)$ expression.

Uncertainty type	$G(z)$
$P = P_n(1+\tilde{\Delta}W)$	$G(z) = \tilde{\Delta}WS$
$P = P_n + \tilde{\Delta}W$	$G(z) = P_n^{-1}\tilde{\Delta}WS$
$P = P_n/(1+\tilde{\Delta}WP_n)$	$G(z) = -\frac{\tilde{\Delta}WP_nS}{1+\tilde{\Delta}WP_n}$
$P = P_n/(1+\tilde{\Delta}W)$	$G(z) = -\frac{\tilde{\Delta}WS}{1+\tilde{\Delta}W}$

oscillations at the output occur at frequency $\omega = \omega_{cr}$. This implies the following:

$$1 + (1 + G(e^{j\omega_{cr}T_s}))\frac{KT_s}{e^{j\omega_{cr}T_s} - 1} = 0 \quad \Rightarrow G\left(e^{j\omega_{cr}T_s}\right) = -1 - \frac{1 - e^{j\omega_{cr}T_s}}{KT_s}. \tag{4}$$

If we restrict the term G such that $\|G\|_\infty < 1$ and force $0 < KT_s < 1$, then the closed loop will be stable and the equality in (4) will not have a real solution for a nonzero ω_{cr}. Following remark summarizes the stability conclusion of our discussion.

Remark: If the uncertainty G has no unstable poles and $\|G\|_\infty < 1$ is satisfied, for any $K > 0$ the closed loop system in Figure 2a is stable if $0 < KT_s < 1$ holds true.

Regarding the final value of $D - \hat{D}$ in Figure 2a, assuming $G(1) > 0$, one can derive the static error constants as $K_p = \lim_{z\to 1}(1+G)\frac{KT_s}{z-1} = \infty$ and $K_v = \lim_{z\to 1}\frac{z-1}{T_s}(1+G)\frac{KT_s}{z-1} = (1+G(1))K$. Apparently, the larger the value of K the better the disturbance prediction performance for ramp-like disturbances.

Aside from the steady state performance issues, we may write the following matrix equation in between the output variables $\{\hat{D}, Y\}$ and the independent input variables $\{D, R, X\}$.

$$\begin{pmatrix} \hat{D} \\ Y \end{pmatrix} = \underbrace{\begin{pmatrix} \mathcal{A}_{11} & \mathcal{A}_{12} \\ \mathcal{A}_{21} & \mathcal{A}_{22} \end{pmatrix}}_{\mathcal{A}} \begin{pmatrix} D \\ R \end{pmatrix} + \underbrace{\begin{pmatrix} \mathcal{B}_1 \\ \mathcal{B}_2 \end{pmatrix}}_{\mathcal{B}} X, \tag{5}$$

where $\mathcal{A}_{11} = \frac{K(1+G)}{\frac{z-1}{T_s}+K(1+G)}$, $\mathcal{A}_{12} = \frac{KGC}{\frac{z-1}{T_s}+K(1+G)}$, $\mathcal{A}_{21} = PS\frac{\frac{z-1}{T_s}}{\frac{z-1}{T_s}+K(1+G)}$, $\mathcal{A}_{22} = T\frac{\frac{z-1}{T_s}+K}{\frac{z-1}{T_s}+K(1+G)}$, $\mathcal{B}_1 = \frac{KN}{\frac{z-1}{T_s}+K(1+G)}$, $\mathcal{B}_2 = -PS\mathcal{B}_1 - T$. Assume $X \equiv 0$ and let the error vector be $\epsilon(e^{j\omega T_s}) := \begin{pmatrix} D(e^{j\omega T_s}) - \hat{D}(e^{j\omega T_s}) \\ R(e^{j\omega T_s}) - Y(e^{j\omega T_s}) \end{pmatrix}$ and the independent external excitation be $\mathcal{F}(e^{j\omega T_s}) := \begin{pmatrix} D(e^{j\omega T_s}) \\ R(e^{j\omega T_s}) \end{pmatrix}$. With these definitions, we can write the following frequency dependent matrix equation:

$$\begin{pmatrix} D(e^{j\omega T_s}) - \hat{D}(e^{j\omega T_s}) \\ R(e^{j\omega T_s}) - Y(e^{j\omega T_s}) \end{pmatrix} = (I - \mathcal{A}(e^{j\omega T_s})) \begin{pmatrix} D(e^{j\omega T_s}) \\ R(e^{j\omega T_s}) \end{pmatrix}. \tag{6}$$

The energy of the error vector at frequency ω and that of the independent external excitation are related to each other as follows:

$$\epsilon^H \epsilon = \mathcal{F}^H \mathcal{M} \mathcal{F}, \tag{7}$$

where ϵ^H is the conjugate transpose of ϵ and $\mathcal{M} := (I-\mathcal{A})^H(I-\mathcal{A})$ and $\mathcal{M}$ is a Hermitian matrix that is dependent upon the frequency, ω. Rayleigh quotient, which quantifies the energy of the error (ϵ) at frequency ω over the energy of the independent excitation signal ($\mathcal{F}$) at that frequency, can now be defined as

$$\frac{\epsilon^H\epsilon}{\mathcal{F}^H\mathcal{F}} = \frac{\mathcal{F}^H\mathcal{M}\mathcal{F}}{\mathcal{F}^H\mathcal{F}} := R(\mathcal{M},\mathcal{F}). \tag{8}$$

Defining $\lambda_{\min}\{\mathcal{M}\}$ and $\lambda_{\max}\{\mathcal{M}\}$ as the smallest and largest eigenvalues of $\mathcal{M}$, respectively, one has the following inequality:

$$\lambda_{\min}\{\mathcal{M}\} \leq R(\mathcal{M},\mathcal{F}) \leq \lambda_{\max}\{\mathcal{M}\}. \tag{9}$$

Ideally, one wants to have $\mathcal{A} = I_{2\times 2}$, $\mathcal{M} = 0_{2\times 2}$ and $\mathcal{B} = 0_{2\times 1}$ and perfect tracking is observed at every frequency, yet this is not the case in practice and it is desired to have small $\lambda_{\max}\{\mathcal{M}\}$ and the values of the eigenvalues of $\mathcal{M}$ depend upon K, P, G and C. This is seen from the entries of the matrix $\mathcal{A}$. An acceptable result would be to obtain $|\mathcal{A}_{11}(e^{j\omega T_s})| \approx 1$, $|\mathcal{A}_{22}(e^{j\omega T_s})| \approx 1$, $|\mathcal{A}_{12}(e^{j\omega T_s})| \ll 1$ and $|\mathcal{A}_{21}(e^{j\omega T_s})| \ll 1$ over the bandwidth of the nominal closed loop transfer function, $T_n := \frac{P_nC}{1+P_nC}$, say $0 \leq \omega \leq \omega_{T_n} < \frac{\pi}{T_s}$.

Finally in this section, we present the implications of $\|G\|_\infty < 1$ on the terms seen in the second column of the table. Since $\|\tilde{\Delta}\|_\infty \leq 1$, one needs $\|WS\|_\infty < 1$ for the first type of uncertainty model, $\|P_n^{-1}WS\|_\infty < 1$ for the second type, $\|\frac{P_nWS}{1+\tilde{\Delta}WP_n}\|_\infty < 1$ for the third type and $\|\frac{WS}{1+\tilde{\Delta}W}\|_\infty < 1$ for the last type of uncertainty described in the table.

In the remaining part of this study, we restrict ourselves to the first type of uncertainty, i.e. $P = P_n(1+\tilde{\Delta}W)$ and leave the other uncertainty types to future studies. The stability condition for $P = P_n(1+\tilde{\Delta}W)$ reduces to the robust stability condition, $\|WS\|_\infty < 1$. The next section describes the proposed modification for the classical Q-filter based loop and a new discontinuous filter, the S-filter, is introduced and the analytical aspects are discussed.

3. Nonlinear DOBC scheme: S-filter based approach

The proposed nonlinear element ($\Phi(.)$) is placed into the DOBC mechanism as shown in Figure 3a. With this modification, the equivalent representation shown in Figure 2a becomes as depicted in Figure 3b. The main issue in the proposed modification is to introduce a nonlinear element that processes the signal E and then the obtained quantity is integrated by the block $\frac{KT_s}{z-1}$ to obtain $\hat{D}$.

In the following discussion, the operator $\star$ denotes the discrete time convolution operator, the subscript k denotes the discrete time index and T_s denotes the sampling period. 1-norm of a causal discrete time signal, say g_k, is computed as $\|g_k\|_1 := \sum_{p=0}^{\infty}|g_p|$.

In the sequel, we give three lemmas that facilitate understanding the contribution of the current paper.

Lemma 1. Let g_k and d_k be discrete time signals defined for $k \geq 0$. $(g_{k+1}-g_k)\star d_k = (d_{k+1}-d_k)\star g_k$ if $d_0 = g_0 = 0$.

Proof 1. Taking the z-transform of both sides and using the properties of z-transform quickly proves.

Lemma 2. Let g_k and e_k be a discrete time signals defined for $k \geq 0$ and let $L > 1$ a constant and $|e_k| \leq \frac{1}{L}$. The quantity $|g_{k+1} \star e_k| \leq \frac{\|g\|_1}{L}$.

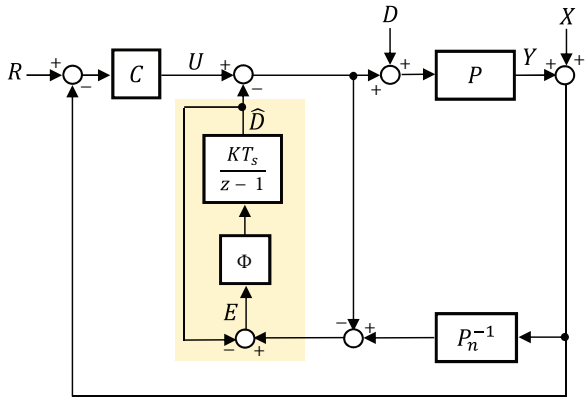

(a) Proposed structure and its equivalent representation.

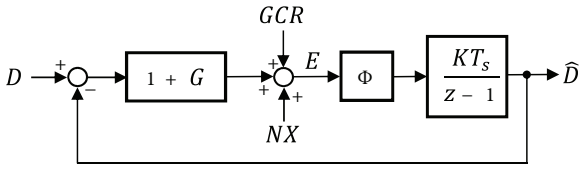

(b) Proposed DOBC block diagram with the nonlinear element Φ. The subsystem in the shaded area is named S-filter, which is sensitive to small magnitude E.

Figure 3. Equivalent representation of the disturbance prediction loop with the nonlinear element Φ.

Proof 2. Following inequalities complete the proof.

$$|g_{k+1} \star e_k| = \left| \sum_{p=0}^{k} g_{k+1-p} e_p \right| \leq \sum_{p=0}^{k} |g_{k+1-p} e_p| \leq \sum_{p=0}^{k} |g_{k+1-p}||e_p| \leq \frac{1}{L} \sum_{p=0}^{k} |g_{k+1-p}| \leq \frac{1}{L} \sum_{p=0}^{\infty} |g_p| = \frac{1}{L} \|g\|_1 \quad (10)$$

Lemma 3. Let g_k and d_k be a discrete time signals defined for $k \geq 0$. Let $F_k := d_k + (g_k \star d_k)$ and let Δ denote the difference, i.e. $\Delta F_k := F_{k+1} - F_k$. It can be shown that $|\Delta F_k| \leq (1 + 2\|g_k\|_1)\mathcal{B}_{\Delta d}$, where $\sup_{k \geq 0} \Delta d := \mathcal{B}_{\Delta d}$

Proof 3. Following inequalities complete the proof.

$$\begin{aligned}
|\Delta F_k| &= |d_{k+1} + (g_{k+1} \star d_{k+1}) - d_k - (g_k \star d_k)| = |d_{k+1} - d_k + (g_{k+1} \star d_{k+1}) - (g_k \star d_k)| \\
&= |\Delta d_k + g_{k+1} \star d_k + g_{k+1} \star \Delta d_k - g_k \star d_k| = |\Delta d_k + (g_{k+1} - g_k) \star d_k + g_{k+1} \star \Delta d_k| \\
&= |\Delta d_k + (d_{k+1} - d_k) \star g_k + g_{k+1} \star \Delta d_k| = |\Delta d_k + g_k \star \Delta d_k + g_{k+1} \star \Delta d_k| \\
&\leq |\Delta d_k| + |g_k + g_{k+1}| \star |\Delta d_k| \leq \mathcal{B}_{\Delta d} + (|g_k| + |g_{k+1}|) \star \mathcal{B}_{\Delta d} \leq (1 + 2\|g_k\|_1)\mathcal{B}_{\Delta d} \qquad (11)
\end{aligned}$$

In the above derivation, we use the result of Lemma 1 while passing from second line to third line.

Theorem 1: Let $e_k := d_k - \hat{d}_k$ be the disturbance prediction error. Let (12) be an update rule for the disturbance prediction dynamics, let $K > 0$, $L > 1$ be gains, and let $\Phi(.)$ be a nonlinear element, whose argument is e_k and the analytical expression of which is as given in (13).

$$\hat{d}_{k+1} := \hat{d}_k + KT_s \Phi(e_k) \quad (12)$$

$$\Phi(e_k) := \begin{cases} \operatorname{sgn}(e_k) & |e_k| \geq 1/L \\ Le_k & |e_k| \leq 1/L \end{cases} \quad (13)$$

Disturbance prediction mechanism proposed above, which is named S-filter, is Lyapunov stable if $K > K_{cr} = \frac{2\|g_k\|_1+1}{2\|g_k\|_1-1}\left(\frac{\mathcal{B}_{\Delta d}}{T_s}\right)$ and $\|g_k\|_1 < \frac{1}{2}$. The absolute value of the error ($|e_k|$) is bounded by $|e_k| \leq \frac{(1+2\|g_k\|_1)}{KL}\left(\frac{\mathcal{B}_{\Delta d}}{T_s}\right) + \frac{2\|g_k\|_1}{L}$.

Proof of Theorem 1: If $(e_{k+1} - e_k)e_k < 0$ is satisfied, then the value of e_k converges to zero as k increases. We will check whether the condition $\Delta V_k := ((\Delta e_k)e_k) = (e_{k+1} - e_k)e_k < 0$ holds true or not.

$$\begin{aligned}
\Delta V_k &= (((d_{k+1} - \hat{d}_{k+1}) + g_{k+1} \star (d_{k+1} - \hat{d}_{k+1})) - ((d_k - \hat{d}_k) + g_k \star (d_k - \hat{d}_k)))e_k && (14)\\
&= (((d_{k+1} - \hat{d}_k - KT_s\Phi(e_k)) + g_{k+1} \star (d_{k+1} - \hat{d}_k - KT_s\Phi(e_k))) - ((d_k - \hat{d}_k) + g_k \star (d_k - \hat{d}_k)))e_k && (15)\\
&= (d_{k+1} - KT_s\Phi(e_k) + g_{k+1} \star (d_{k+1} - \hat{d}_k - KT_s\Phi(e_k)) - d_k - g_k \star (d_k - \hat{d}_k))e_k && (16)\\
&= ((d_{k+1} + g_{k+1} \star d_{k+1}) - (d_k + g_k \star d_k) - KT_s\Phi(e_k) + g_{k+1} \star (-\hat{d}_k - KT_s\Phi(e_k)) - g_k \star (-\hat{d}_k))e_k && (17)\\
&= (F_{k+1} - F_k - KT_s\Phi(e_k) - g_{k+1} \star (\hat{d}_k + KT_s\Phi(e_k)) + g_k \star \hat{d}_k)e_k && (18)\\
&= (\Delta F_k - KT_s\Phi(e_k) - (g_{k+1} - g_k) \star \hat{d}_k - g_{k+1} \star KT_s\Phi(e_k))e_k && (19)\\
&= (\Delta F_k - KT_s\Phi(e_k) - \Delta g_k \star \hat{d}_k - g_{k+1} \star KT_s\Phi(e_k))e_k && (20)
\end{aligned}$$

According to Lemma 1, $\Delta g_k \star \hat{d}_k = \Delta \hat{d}_k \star g_k$ and from (12) we know that $\Delta \hat{d}_k = \hat{d}_{k+1} - \hat{d}_k = KT_s\Phi(e_k)$. Using this relation, we can continue from (20) as

$$\Delta V_k = \Delta F_k e_k - KT_s\Phi(e_k)e_k - KT_s((g_k + g_{k+1}) \star \Phi(e_k))e_k. \quad (21)$$

We will continue the analysis for two different cases, i) $|e_k| \geq \frac{1}{L}$ and according to (13), $\Phi(e_k) = \text{sgn}(e_k)$, and ii) $|e_k| \leq \frac{1}{L}$ that requires $\Phi(e_k) = Le_k$.

Case 1: $|e_k| \geq \frac{1}{L}$, Inserting $\Phi(e_k) = \text{sgn}(e_k)$ into (21) results in

$$\begin{aligned}
\Delta V_k &= \Delta F_k e_k - KT_s|e_k| - KT_s((g_{k+1} + g_k) \star \text{sgn}(e_k))e_k && (22)\\
&= \Delta F_k e_k - KT_s|e_k| - KT_s((g_{k+1} + g_k) \star 1)|e_k| && (23)\\
&\leq |\Delta F_k||e_k| - KT_s|e_k| + 2KT_s\|g\|_1|e_k| && (24)\\
&\leq (|\Delta F_k| - KT_s + 2KT_s\|g\|_1)\,|e_k| && (25)
\end{aligned}$$

Using the result of Lemma 3, we can continue from (25) as

$$\Delta V_k \leq ((1 + 2\|g_k\|_1)\mathcal{B}_{\Delta d} - KT_s + 2KT_s\|g_k\|_1)\,|e_k| \quad (26)$$

which requires $K > \frac{1+2\|g_k\|_1}{1-2\|g_k\|_1}\left(\frac{\mathcal{B}_{\Delta d}}{T_s}\right) := K_{cr}$ for $\Delta V_k < 0$. Since $K > 0$, the result obtained here entails $\|g_k\|_1 < \frac{1}{2}$ and since $0 < KT_s < 1$ is needed, this inequality further requires $\mathcal{B}_{\Delta d} < \frac{1-2\|g_k\|_1}{1+2\|g_k\|_1}$.

Case 2: $|e_k| \leq \frac{1}{L}$, Inserting $\Phi(e_k) = Le_k$ into (21) results in

$$\begin{aligned}
\Delta V_k &= \Delta F_k e_k - KT_sL|e_k|^2 - KT_sL((g_k + g_{k+1}) \star e_k)e_k && (27)\\
&\leq |\Delta F_k||e_k| - KT_sL|e_k|^2 + KT_sL|(g_k + g_{k+1}) \star e_k||e_k| && (28)
\end{aligned}$$

Since $|e_k| \leq \frac{1}{L}$, using the definition of the convolution, we can write $|g_k \star e_k| \leq \frac{\|g_k\|_1}{L}$ and $|g_{k+1} \star e_k| \leq \frac{\|g_k\|_1}{L}$ and continue from (28) as

$$\begin{aligned} \Delta V_k &\leq |\Delta F_k||e_k| - KT_sL|e_k|^2 + 2KT_sL\frac{\|g_k\|_1}{L}|e_k| && (29)\\ &\leq (1+2\|g_k\|_1)\mathcal{B}_{\Delta d}|e_k| - KT_sL|e_k|^2 + 2KT_s\|g_k\|_1|e_k| && (30)\\ &= ((1+2\|g_k\|_1)\mathcal{B}_{\Delta d} + 2KT_s\|g_k\|_1)\,|e_k| - KT_sL|e_k|^2 && (31)\end{aligned}$$

The expression in (31) bounds the absolute value of the error ($|e_k|$) by

$$|e_k| \leq \frac{(1+2\|g_k\|_1)}{KL}\left(\frac{\mathcal{B}_{\Delta d}}{T_s}\right) + \frac{2\|g_k\|_1}{L} \tag{32}$$

Corollary 1. As $L \to \infty$, we observe $\Phi(e_k) \to \text{sgn}(e_k)$ and this fact motivates the designer to choose finitely large L, which leads to narrow transition region around $|e_k| \approx 0$.

Corollary 2. Let $\alpha > 1$ and set $K = \alpha K_{cr}$. Inserting this value into the bound expression in (32) yields $|e_k| \leq \frac{1+2\|g_k\|_1(\alpha-1)}{\alpha L}$. A special case is obtained when $\alpha = 1$, which leads to $|e_k| \leq \frac{1}{L}$ as $\|g_k\|_1$ is bounded by $\frac{1}{2}$.

Corollary 3. The quantity $\frac{\mathcal{B}_{\Delta d}}{T_s}$ is a numerical approximate of the time derivative of the continuous time disturbance signal. Apparently, for a better disturbance prediction performance, the practicing engineer must consider applications where the disturbance signal has a bounded derivative. This is an underlying fact for all DOBC mechanisms and utilizing $0 < KT_s < 1$, the presented approach puts an upper bound to this quantity as $\mathcal{B}_{\Delta d} < \frac{1-2\|g_k\|_1}{1+2\|g_k\|_1}$.

In order to compare the classical approach with the proposed scheme, we will study the quasilinear representation of the introduced nonlinearity and consider its describing function as given in (33), where the term A^* stands for the magnitude of the oscillations at the input of the nonlinear element.

$$\mathcal{N}(A^*) = \begin{cases} L & A^* \leq 1/L \\ \frac{2L}{\pi}\left(\sin^{-1}\left(\frac{1}{LA^*}\right) + \frac{1}{LA^*}\sqrt{1-\frac{1}{(LA^*)^2}}\right) & A^* > 1/L \end{cases} \tag{33}$$

Corollary 4. The term $\mathcal{N}(A^*)$ joins the loop as a gain, and for the proposed approach, this changes the stability requirement on the gain K as $0 < KT_s\max\{\mathcal{N}(\mathrm{A}^*)\} < 1$, i.e. we have the following inequality.

$$0 < KLT_s < 1 \tag{34}$$

Corollary 5. The inequality in (34) requires finite L, i.e. one cannot choose $\Phi(e_k) = \text{sgn}(e_k)$ as $\mathcal{N}(A^*)$ for this case would not be bounded for small A^*.

Considering (5) by setting $X \equiv R \equiv 0$, we can write the transfer function $\frac{\hat{D}(z)}{D(z)}$ for the classical scheme as in (35) and for the proposed scheme as in (36).

$$T_Q(z) = \frac{K(1+G)}{\frac{z-1}{T_s} + K(1+G)} \tag{35}$$

$$T_S(z) = \frac{\mathcal{N}(A^*)K(1+G)}{\frac{z-1}{T_s} + \mathcal{N}(A^*)K(1+G)} \tag{36}$$

We would like to investigate the energy of the disturbance prediction error defined as $\varepsilon := \sqrt{\int_0^\infty (d(t) - \hat{d}(t))^2 \mathrm{d}t}$. Due to the Parseval's theorem, it is possible to express the energy equation as $\varepsilon := \sqrt{\frac{1}{2\pi}\int_{-\infty}^{\infty} |D(e^{j\omega T_s}) - \hat{D}(e^{j\omega T_s})|^2 \mathrm{d}\omega}$. Define $Z(e^{j\omega T_s}) := \frac{e^{j\omega T_s}-1}{T_s}$ and define the disturbance prediction signal for the proposed scheme as $\hat{D}_S(z) := T_S(z)D(z)$ and that for the classical mechanism in Figure 1b as $\hat{D}_Q(z) := T_Q(z)D(z)$. This would let us write the following energy equations for each case.

$$\varepsilon_Q^2 = \frac{1}{2\pi}\int_{-\infty}^{\infty} \frac{|D(e^{j\omega T_s})|^2 |Z(e^{j\omega T_s})|^2}{|Z(e^{j\omega T_s}) + K(1+G)|^2} \mathrm{d}\omega \tag{37}$$

$$\varepsilon_S^2 = \frac{1}{2\pi}\int_{-\infty}^{\infty} \frac{|D(e^{j\omega T_s})|^2 |Z(e^{j\omega T_s})|^2}{|Z(e^{j\omega T_s}) + \mathcal{N}(A^*)K(1+G)|^2} \mathrm{d}\omega \tag{38}$$

Since the numerators of (37) and (38) are the same, the denominators will determine the result, on which the term $\mathcal{N}(A^*)$ will be effective. The goal of the approach presented here is to obtain a good prediction for the disturbance $d(t)$ within the bandwidth of the nominal control system, therefore, we will consider the quantities shown above within an acceptable neighborhood of the bandwidth.

In order to understand the denominators of the above quantities, define $l_Q := \left|Z(e^{j\omega T_s}) + K(1+G)\right|$ and $l_S := \left|Z(e^{j\omega T_s}) + \mathcal{N}(A^*)K(1+G)\right|$. In Figure 4, the possible set of locations for G is shown in subplot (a). Figure 4b shows the translation of G by unity, and Figure 4c illustrates the set for $K(1+G)$. In the classical case, where there is no nonlinear element, we obtain the set shown in Figure 4d, where the magnitude of a point is denoted by l_Q. In Figure 4e, the loci obtained for the quantity $Z(e^{j\omega T_s}) + \mathcal{N}(A^*)K(1+G)$ is added. If $\mathcal{N}(A^*) > 1$, the new set is away from the origin compared to the case shown in subplot (d).

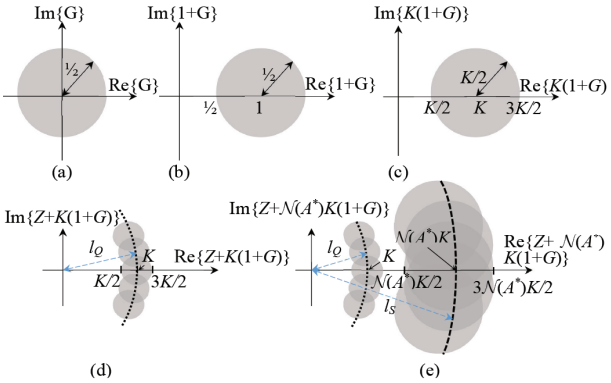

Figure 4: Possible loci for the quantity $Z(e^{j\omega T_s}) + K(1+G)$ and $Z(e^{j\omega T_s}) + \mathcal{N}(A^*)K(1+G)$.

Since $\mathcal{N}(A^*) = L$ for $A^* \leq \frac{1}{L}$ and since $L > 1$ (see Theorem 1), we can conclude that for small magnitude oscillations $\mathcal{N}(A^*) = L > 1$ and the deployment shown in Figure 4e is observed and the disturbance

prediction loop becomes sensitive to small magnitude inputs which enhances the loop performance in terms of the energies defined in (37) and (38), i.e. we obtain $\varepsilon_S < \varepsilon_Q$, which is desired. In the following section, we present a numerical example.

4. Simulation results

In this section, we present an exemplar case justifying the theoretical claims of the previous section. We consider type-0 biproper system with the sampling period is $T_s = 2$ sec. Since the nominal model is stable and biproper, its inverse is causal and the system is physically realizable. These are given as follows: $P_n(z) = \frac{z^2}{(z-0.8)(z-0.1)}$, $P_n^{-1}(z) = \frac{(z-0.8)(z-0.1)}{z^2}$. We follow the dead-beat control scheme for the nominal control system, i.e. $T_n = z^{-1}$, and the digital controller $C(z)$, is obtained as $C(z) = \frac{T_n}{(1-T_n)P_n^{-1}} = \frac{(z-0.8)(z-0.1)}{z^2(z-1)}$.

Lemma 1 requires $g_0 = 0$ and we consider the set of uncertainties that contain pure delay, and we choose $\tilde{\Delta}(z) = 0.1z^{-1} + 0.2z^{-2} + 0.125z^{-3}$ and $W(z) = 1$, which satisfy the requirements $\|g_k\|_1 = 0.2959 < \frac{1}{2}$ and $\|G\|_\infty = 0.4563 < 1$. The choice of pure delay in $\tilde{\Delta}(z)$ is deliberate as it is the most common difficulty in industrial control systems.

Due to the dead-beat property, the controller above provides a fast response displaying no overshoot for the nominal model. During the simulations, we set $L = 4$. Choosing a smaller L would make the system behave as if there was no nonlinearity, yet larger values of L might provoke undesired oscillations. Since $T = 2$ sec. the allowable gain for gain K is $0 < K < 0.5$ and we set $K = 0.124$, which also satisfies the inequality (34). For the given $P_n(z)$ and $C(z)$, the bandwidth of the nominal control system is practically infinity yet the bandwidth of the nominal model (ω_{P_n}) is finite and we adopt $\omega_{T_n} := \omega_{P_n} \approx 1.11$ rad/sec to obtain a good closed loop performance within the bandwidth of the nominal plant model.

In Figure 5a, Bode magnitude plots of the entries of the matrix $\mathcal{A}$ of (5) are shown for $\omega \in [0,\ 1.11]$ rad/sec. As desired, $\mathcal{A}_{11}$ and $\mathcal{A}_{22}$ display a lowpass characteristic. The low frequency gains are very close to unity within the bandwidth of the nominal control system. The terms $\mathcal{A}_{12}$ and $\mathcal{A}_{21}$ are fairly suppressed for low frequencies and $\mathcal{A}_{21}$ becomes effective as the frequency increases, and this is an expected result.

In Figure 5b, Bode magnitude plots of the matrices $\mathcal{B}$, GC and N are depicted. One should note that choosing another $C(z)$ that provides quicker transient response would increase the controller gain and the terms seen in Figure 5b are influenced adversely. Ideally we desire $\mathcal{B} \approx 0$, if this is not possible, small values are preferable.

The eigenvalues of the Rayleigh quotient defined in (8) are depicted in the top subplot of Figure 6a, where we see from the top subplot that $\lambda_{\max}\{\mathcal{M}\}$ is acceptably small when $\omega \ll \omega_{T_n}$. This means that the energy of the error signal (ϵ) is smaller than the energy of the external excitations ($\mathcal{F}$). The bottom subplot of Figure 6a depicts the Nyquist plot of $G(e^{j\omega T_s}) = \tilde{\Delta}(e^{j\omega T_s})W(e^{j\omega T_s})S(e^{j\omega T_s})$. The figure reveals that $\|G\|_\infty = 0.4563 \leq 0.5$ and for the given quantities, we compute $\|g_k\|_1 = 0.2959 < 0.5$.

In Figure 6b, we first compare the quantities $l_Q := \left|Z(e^{j\omega T_s}) + K(1+G)\right|$ and $l_S := \left|Z(e^{j\omega T_s}) + \mathcal{N}(A^*)K(1+G)\right|$ as shown in Figure 4. Nine different K values are considered and the values are chosen to be logarithmically spaced in between 0.01 and 0.124. In each subplot of Figure 6b, we depict the value of l_Q and l_S. While producing the curve for l_S, we consider one hundred A^* values that are logarithmically spaced in between 10^{-4} and $1/L$, and obtain the value of $\mathcal{N}(A^*)$ and calculate

$l_S := \left|Z(e^{j\omega T_s}) + \mathcal{N}(A^*)K(1+G)\right|$. The plotted l_S curve represents the worst case that can be encountered at each frequency. As can be seen from the figure, the proposed approach produces larger l_S values resulting in smaller energy especially for low frequencies.

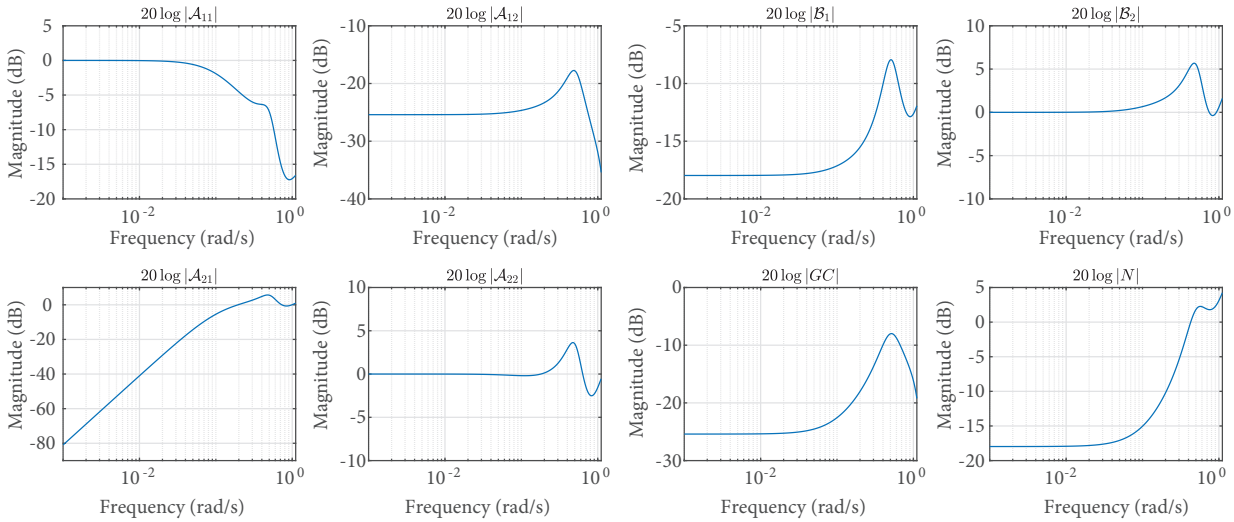

(a) Magnitude plots of the entries of matrix $\mathcal{A}$.

(b) Magnitude plots of the entries of terms $\mathcal{B}$, GC and N.

Figure 5. Magnitude plots of the relevant quantities.

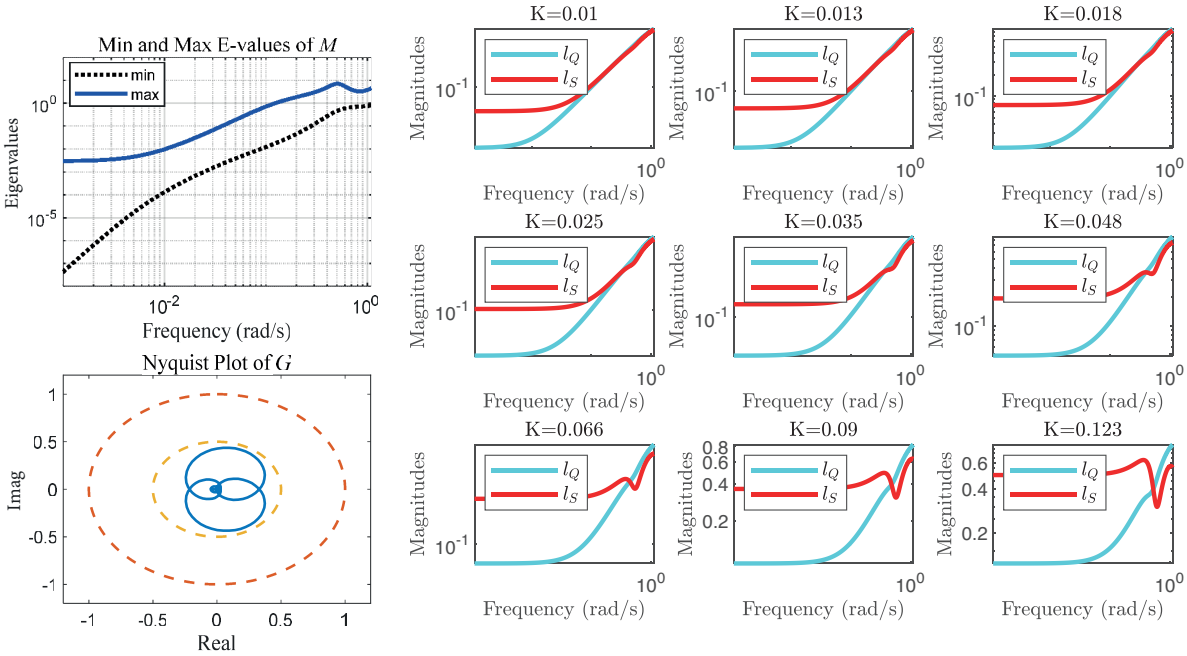

(a) Top: eigenvalues of the matrix $\mathcal{M}$. Bottom: Nyquist plot of the term G.

(b) The values of l_Q and l_S over the frequency axis.

Figure 6. Observations on uncertainty and energy comparison

In Figure 7a, time domain results are illustrated. The response of the closed loop system is desired to follow a sinusoidal signal, a square wave signal and a sawtooth signal to see the tracking ability of the closed loop system. The plant output is contaminated by Gaussian noise (signal X in Figure 3a) with variance equal to $1e-5$. A disturbance signal, shown in the second subplot of Figure 7a, containing a mixture of a chirp and Gaussian noise with variance $1e-3$ is applied as d. The tracking errors are shown in the third subplot, where we see that the proposed modification produces smaller tracking errors and the disturbance prediction errors, $d-\hat{d}_Q$ and $d-\hat{d}_S$, are illustrated in the bottom subplot of Figure 7a, where it is clearly seen that the proposed mechanism produces a considerably smaller prediction error thereby leading to a smaller energy as expected.

The control signals produced in both cases and the energy values for the considered simulation studies are depicted in Figure 7b. The top subplot shows the control signals, where we see that the control effort for the proposed mechanism is visibly lower than the case that does not use the nonlinear term. The tracking error energies are compared in the middle subplot and the disturbance prediction error energies are compared in the bottom subplot. The given results emphasize that the introduced nonlinear term in Figure 3a improves the performance of the control system significantly. However, choosing larger K values deteriorates the performance and the energy efficient property is lost as K approaches the allowable limit, which is 0.5 in our simulations.

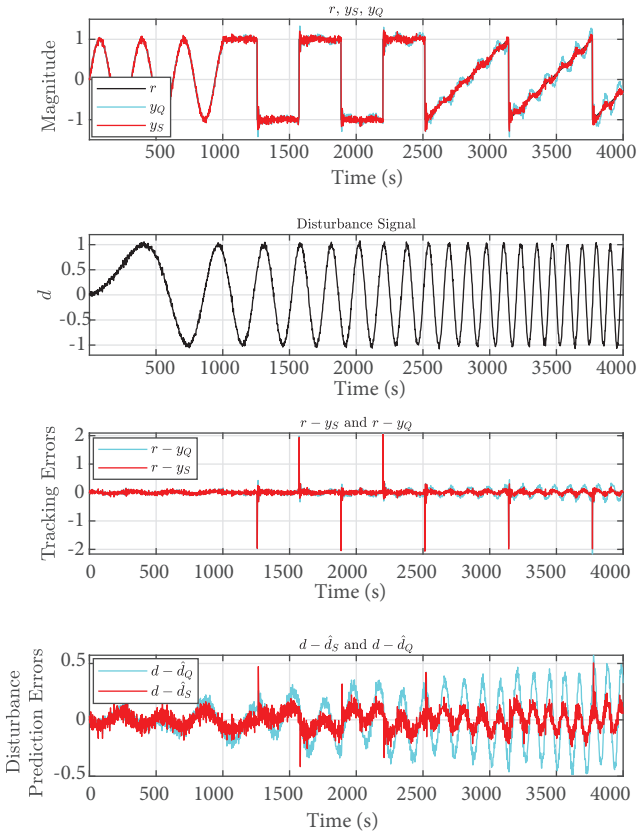

(a) Time domain simulation results.

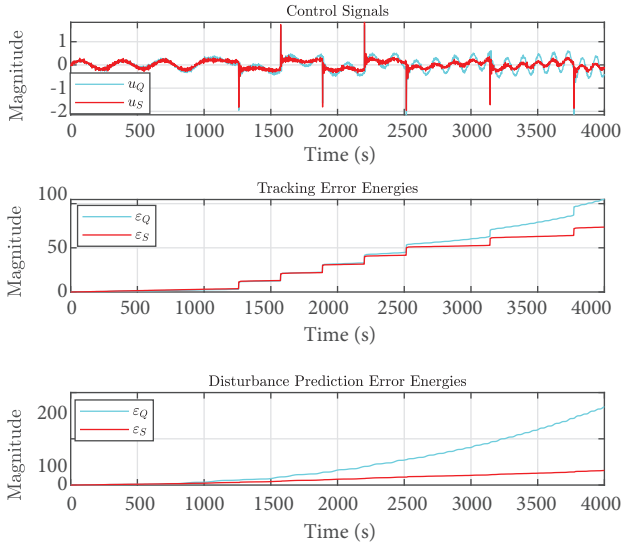

(b) Top: control signals. Middle: energies of the tracking errors. Bottom: energies of the disturbance prediction errors.

Figure 7. Simulation results

In Figure 8a, the deployment of the terms $Z(e^{j\omega T_s}) + K(1+G)$ and $Z(e^{j\omega T_s}) + \mathcal{N}(A^*)K(1+G)$ are depicted for the chosen parameter values. We choose four different $\mathcal{N}(A^*)$ values, which correspond to choosing $L = 1, 2, 3, 4$, and draw the above terms. The locations coincide when $\mathcal{N}(A^*) = 1$ as shown in the top left subplot. When the value of $\mathcal{N}(A^*)$ is increased gradually it is seen that the low frequency performance is influenced positively and all possible l_S values become larger than the l_Q values as the frequency runs from zero to $\omega_{T_n} \approx 1.11$ rad/s.

In Figure 8b, we illustrate the curve that determines the maximal $\mathcal{B}_{\Delta d}$ on the left. In the simulations, we compute $\mathcal{B}_{\Delta d} = 0.24 < \frac{1-2\|g_k\|_1}{1+2\|g_k\|_1} = 0.2564$. In the right subplot of Figure 8b, the error bound surfaces that occur for different values of L are shown. Uppermost sheet is for the case $L = 1$, and the lowest sheet is for the case where $L = 4$. Clearly increasing L has a positive effect on the error bound yet such a case would provoke the undesired oscillations as the nonlinearity $(\Phi(.))$ approaches the signum function.

Lastly, we show the disturbance prediction performance when the command signal (r) is zero. A small magnitude noiseless chirp signal shown in the left subplot is applied and the results seen in Figure ?? are obtained. The middle and right subplots reveal that the tracking errors and the disturbance prediction errors are smaller in magnitude for all frequencies contained in the applied chirp type disturbance signal.

This observation lets us conclude that the disturbance selectivity of the proposed technique is better than its classical counterpart for all frequencies contained in the applied chirp disturbance.

5. Conclusion

This paper presents a nonlinear disturbance observer scheme for discrete time systems. The original algorithm is reconsidered in terms of stability and performance aspects. The lowpass filter of the classical approach is implemented in a feedback form together with a nonlinear component. Necessary stability conditions are derived and the theoretical claims have been justified on a discrete time system having some uncertainty. Simulations show that the proposed technique is successful in predicting the disturbance signal when the disturbance prediction error energies are compared with the classical scheme. This paper contributes to the literature in terms of the following aspects: i) The continuous time DOBC scheme is discretized and the conditions for stability are derived. ii) The discrete time setting is improved by introducing a nonlinear element that makes the disturbance observer subsystem sensitive to small signals as $L > 1$. iii) Necessary conditions for stability are derived and robustness properties are analyzed. iv) An enhanced performance is observed with minor modification to the classical approach.

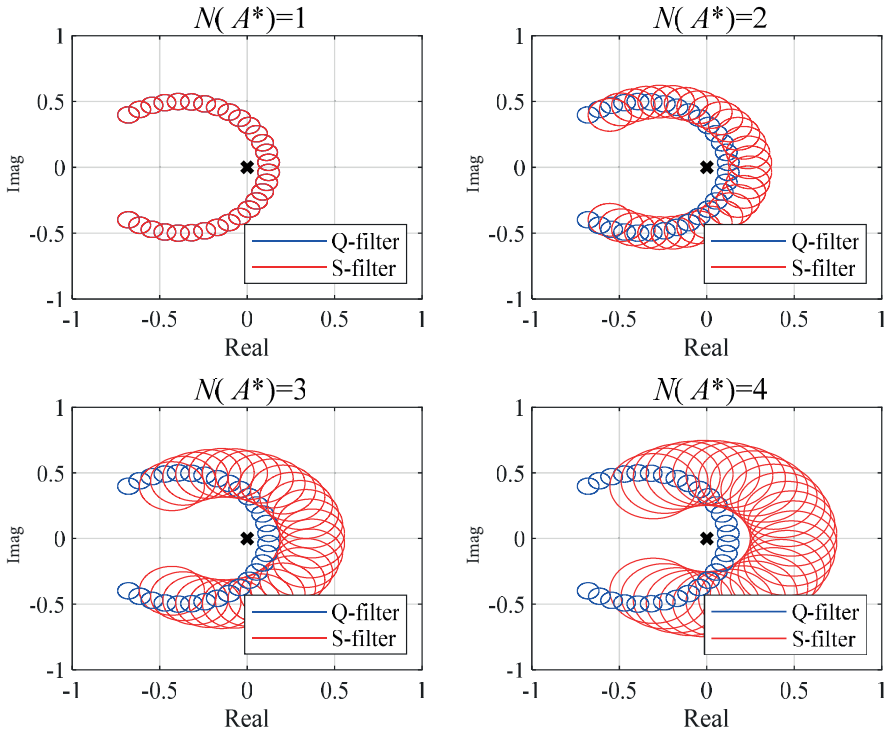

(a) The deployment of the uncertainty terms.

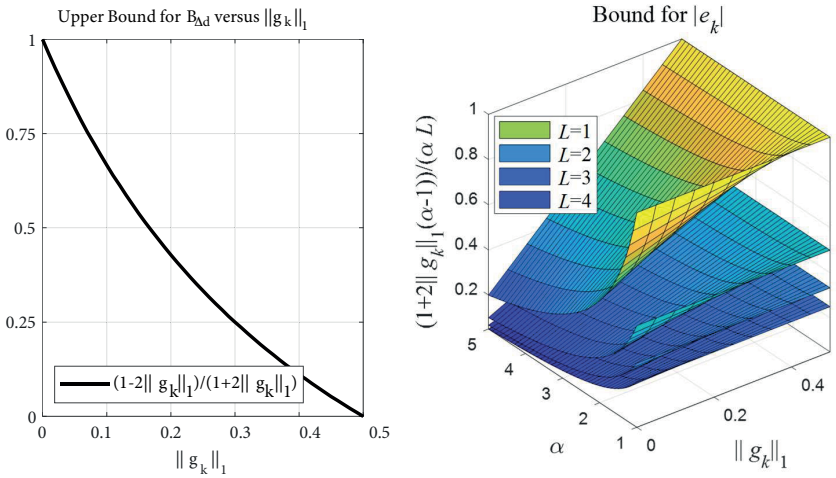

(b) Left: the bound for $\mathcal{B}_{\Delta d}$ versus $\|g_k\|_1$. Right: the error bound surfaces for different α, $\|g_k\|_1$ and L.

Figure 8. Simulation results.

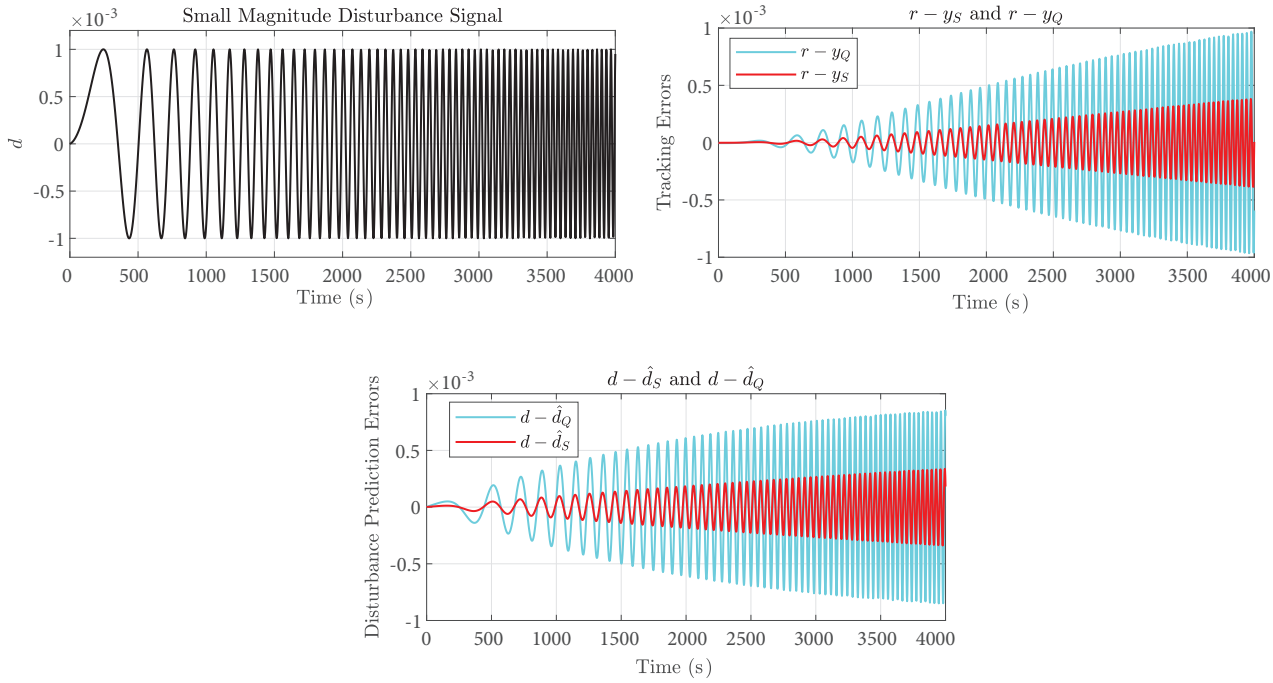

Figure 9. The results when the disturbance is a chirp signal and the command signal is zero ($r = 0$).

References

[1] Gürhanlı A. Modified acceleration feedback for practical disturbance rejection in motor drives. Turkish Journal of Electrical Engineering & Computer Sciences 2018; 26: 2151-2161.

[2] Vatankhah B, Farrokhi M. Offset-free adaptive nonlinear model predictive control with disturbance observer for DC-DC buck converters. Turkish Journal of Electrical Engineering & Computer Sciences 2017; 25: 2195-2206.

[3] Zeinaly Z, Ramezani A, Ozgoli S. Design and implementation of a modified communication disturbance observer for teleoperation systems. Turkish Journal of Electrical Engineering & Computer Sciences 2017; 25: 1522-1540.

[4] Ohishi K, Ohnishi K, Miyachi K. Torque-speed regulation of dc motor based on load torque estimation method. In: Proceedings of the JIEE International Power Electronics Conference; Tokyo, Japan; 1983. pp. 1209-1218.

[5] Chen WH, Yang J, Guo L, Li S. Disturbance-observer-based control and related methods-an overview. IEEE Transactions on Industrial Electronics 2016; 63 (2): 1083-1095.

[6] Sarıyıldız E, Oboe R, Ohnishi K. Disturbance observer-based robust control and its applications: 35th anniversary overview. IEEE Transactions on Industrial Electronics 2019; 67 (3): 2042-2053.

[7] Kempf CJ, Kobayashi S. Discrete-time disturbance observer design for systems with delay. In: Proceedings of 4th IEEE International Workshop on Advanced Motion Control; Mie, Japan; 1996. pp. 332-337.

[8] Godler I, Honda H, Ohnishi K. Design guidelines for disturbance observer's filter in discrete time. In: Proceedings of 7th IEEE International Workshop on Advanced Motion Control; Maribor, Slovenia; 2002. pp. 390-395.

[9] Yang K, Choi Y, Chung WK. Performance analysis of discrete-time disturbance observer for second-order systems. In: Proceedings of the 42nd IEEE Conference on Decision and Control; Maui, Hawaii, USA; 2003. pp. 4877-4882.

[10] Chen C, Tomizuka M. Optimal plant shaping for high bandwidth disturbance rejection in discrete disturbance observers. In: American Control Conference; Baltimore, MD, USA; 2010. pp. 2641-2646.

[11] Lee C, Joo Y, Shim H. Analysis of discrete-time disturbance observer and a new q-filter design using delay function. In: 12th International Conference on Control, Automation and Systems; Jeju Island, Korea; 2012. pp. 556-561.

[12] Kang D. Design of a disturbance observer for discrete-time linear systems. In: 14th International Conference on Control, Automation and Systems; Gyeonggi-do, Korea; 2014. pp. 1381-1383.

[13] Park G. Joo Y, Lee C, Shim H. On robust stability of disturbance observer for sampled-data systems under fast sampling: an almost necessary and sufficient condition. In: IEEE 54th Annual Conference on Decision and Control; Osaka, Japan; 2015. pp. 7536-7541.

[14] Shim H, Jo NH. An almost necessary and sufficient condition for robust stability of closed-loop systems with disturbance observer. Automatica 2009; 45 (1): 296-299.

[15] Yun H, Park G, Shim H, Chang HJ. State-space analysis of discrete-time disturbance observer for sampled-data control systems. In: American Control Conference; Boston, MA, USA; 2016. pp. 4233-4238.

[16] Uzunovic T, Sariyildiz E, Sabanovic A. A discussion on discrete implementation of disturbance-observer-based control. In: IEEE 15th International Workshop on Advanced Motion Control; Tokyo, Japan 2018. pp. 613-618.

[17] Muramatsu H, Katsura S. An adaptive periodic-disturbance observer for periodic-disturbance suppression. IEEE Transactions on Industrial Informatics 2018; 14 (10): 4446-4456.